

Spectral mechanism and nearly reducible transfer matrices for pseudotransitions in one-dimensional systems

Onofre Rojas

Department of Physics, Institute of Natural Science, Federal University of Lavras, Lavras, MG, Brazil

Abstract

While true phase transitions are forbidden in one-dimensional systems with short-range interactions, several models have recently been shown to exhibit sharp yet analytic thermodynamic anomalies that mimic thermal phase transitions. We show that this behavior arises from transfer matrices that are mathematically irreducible but possess a nearly block-diagonal structure due to the weak contribution of off-diagonal Boltzmann weights in the low-temperature regime. This results in weakly coupled competing sectors whose eigenvalue competition produces abrupt crossovers without nonanalyticity, a mechanism we term nearly block-diagonal irreducible. A key thermodynamic signature of such pseudotransitions is that the residual entropy at the interface remains bounded between the residual entropies of the competing sectors. We develop a general spectral framework to describe this behavior and apply it to two representative models: the Ising chain with internal degeneracy (Doniach model) and a hexagonal nanowire chain with mixed spin-1/2 and spin-1 components. In the first case, we derive exact expressions for the pseudo-critical temperature and residual entropy. In the second, we reduce the full 1458×1458 transfer matrix via symmetry decomposition and construct a low-rank effective matrix that accurately captures the crossover between quasi-ferromagnetic and quasi-core-ferromagnetic regimes. Our results demonstrate that pseudotransitions can be understood as spectral phenomena emerging from irreducible but functionally decoupled structures within the transfer matrix.

Keywords: Pseudotransitions; Avoided level crossing; Residual entropy; Nearly reducible matrices

1. Introduction

The absence of thermodynamic phase transitions in one-dimensional (1D) systems with short-range interactions is well established through rigorous results, including the van Hove theorem [1, 2] and its generalization by Cuesta and Sánchez [3]. These theorems demonstrate the analyticity of the free energy under conditions of homogeneity and finite-range interactions. The argument relies on properties of the transfer matrix, which, under the Perron-Frobenius theorem [4, 5, 6], must be irreducible and strictly positive. This ensures a unique, non-degenerate dominant eigenvalue, thereby precluding non-analytic behavior in thermodynamic potentials [3, 6].

Despite this prohibition, a growing body of work over the past decade has reported thermodynamic anomalies in 1D models that closely resemble true phase transitions. These features include sharp but continuous changes in entropy and internal energy, along with pronounced peaks in specific heat or susceptibility near certain temperatures. Although the free energy remains analytic, the resulting behavior strongly mimics both first- and second-order transitions, raising questions about the origin and interpretation of such anomalies [7, 8, 9].

These anomalies tend to occur at specific temperatures and closely resemble finite-size effects seen in simulations, such as the sharp peaks in observables from Monte Carlo studies on finite lattices [10]. This similarity has led to the adoption of the term pseudotransition to describe such behavior. Timonin [11],

in his study of spin ice under an external field, used similar terminology to refer to these sharp anomalies and introduced the concept of quasi-phases to describe the regions where they arise. Since then, the term has gained traction in describing these 1D anomalies [12], although this feature is sometimes referred to as an ultranarrow phase crossover or a forbidden phase transition [13, 14, 15, 16, 17, 18].

One important line of investigation concerns the apparent universality of these anomalies. In several models, they have been characterized by a consistent set of pseudo-critical exponents: the specific heat scales with $\alpha = 3$, the correlation length with $\nu = 1$, and the susceptibility with $\gamma = 3$, suggesting a degree of universality in their thermodynamic behavior [19]. Ref. [20] further supports this picture by analyzing finite-size effects near the anomaly, showing how the observed behavior sharpens with system size. Other studies have explored the role of residual entropy near the anomalous region, revealing additional thermodynamic signatures [21]. Recent analyses of diluted Ising chains under constrained thermodynamic potentials, such as fixed density, reveal that pseudo-critical exponents and entropy-based criteria are not preserved [22], although the anomalies remain evident.

Correlation functions are central to understanding pseudotransitions in one-dimensional spin systems, as they reveal the emergence of extended short-range order despite the absence of true criticality. In exactly solvable models such as the Ising-Heisenberg and Ising-XYZ diamond chains, the correlation length

exhibits a sharp but finite peak at the pseudo-critical temperature [23, 24]. Similar behavior has been observed in q -state Potts-like chains [25]. This phenomenon arises from a near-degeneracy of subleading eigenvalues in the transfer matrix, leading to a bifurcation in the correlation length a key spectral signature of pseudotransitions [26]. The resulting slow decay of correlations reflects a large but finite correlation length, reinforcing the view of these anomalies as remnants of forbidden phase transitions in low dimensions.

Over the past decade, numerous models have been shown to exhibit such behavior. These include the Ising chain with internal degeneracy [27], the Ising diamond chain [28, 29], and more elaborate systems like the spin-1/2 Ising-Heisenberg diamond chain and its variants, which display pseudotransitions near ground-state boundaries [19, 24, 30]. The diluted Ising chain studied by Panov links the anomaly to residual entropy at critical interfaces [22, 31, 32]. Other examples include double-tetrahedral chains with mixed spins in external fields [33], as well as triangular and ladder Ising-Heisenberg models [26, 30, 34], many of which can be mapped to simpler effective systems via decoration transformation. In most cases, the effective transfer matrices reduce to sizes such as 2×2 [12] or 4×4 , as in the extended Hubbard chain in atomic limit [35, 36]. More complex cases include a 6×6 matrix in spin-pseudospin cuprate models [37], an 8×8 matrix in the Toblerone-like Ising chain [26], and a 92×92 irreducible matrix in the Blume-Capel nanowire model [38], as well as general $q \times q$ matrices in Potts-like chains [25, 39].

In this work, we propose a unified framework to understand the origin of pseudotransitions in one-dimensional systems through the lens of transfer matrix structure. Sec.2 motivates the phenomenon from known examples and ensemble sensitivity. Sec.3 develops the central spectral theory, identifying nearly reducible matrices as the key mechanism behind sharp but analytic crossovers. This includes explicit spectral criteria, correlation length scaling, and thermodynamic implications. Sec.4 and 5 apply this framework to two representative models: an Ising chain with internal degeneracy (Doniach model [40]) and a mixed-spin nanowire system, respectively. We conclude in Sec.6 by discussing thermodynamic signatures and directions for future generalizations.

2. Transfer matrix and matrix structure

The transfer matrix technique in statistical physics was introduced in 1941 by H. Kramers and G. Wannier [41]. Since then, it has been widely used to compute the partition functions of several lattice models. In this approach, the partition function is expressed as a sum over all microstates, with each term weighted by the Boltzmann factor corresponding to the energy of that state.

2.1. Transfer matrix and irreducibility

Consider a general non-symmetric transfer matrix $\mathbf{V} \in \mathbb{R}^{n \times n}$ with non-negative entries $v_{i,j} \geq 0$, written as

$$\mathbf{V} = \begin{pmatrix} v_{1,1} & v_{1,2} & \cdots & v_{1,n} \\ v_{2,1} & v_{2,2} & \cdots & v_{2,n} \\ \vdots & \vdots & \ddots & \vdots \\ v_{n,1} & v_{n,2} & \cdots & v_{n,n} \end{pmatrix}. \quad (1)$$

A key mathematical concept is the irreducibility of the transfer matrix. A non-negative matrix \mathbf{V} is said to be irreducible if it cannot be brought into block upper-triangular form via simultaneous permutations of rows and columns. Physically, irreducibility ensures full connectivity between microscopic configurations across the chain.

In order to analyze the eigenvalues of the matrix \mathbf{V} , we use the Perron-Frobenius theorem [4, 5, 6].

Theorem 1. [Perron-Frobenius] *Let $\mathbf{V} \in \mathbb{R}^{n \times n}$ be a non-negative, irreducible matrix. Then:*

- *There exists a unique largest eigenvalue $\lambda_1 > 0$, which is simple (non-degenerate);;*
- *the corresponding right eigenvector $|\psi\rangle$ has strictly positive components, i.e., $\langle i|\psi\rangle > 0$ for all $i = 1, \dots, n$;*
- *and all other eigenvalues λ_j satisfy $|\lambda_j| < \lambda_1$, $j = 2, \dots, n$.*

In statistical mechanics, this theorem guarantees that in the thermodynamic limit, the partition function is dominated by a single, positive eigenvalue λ_1 , which controls the free energy per site. This ensures the system has a well-defined thermodynamic behavior without degeneracies.

However, to fully exclude phase transitions, one must also ensure that the leading eigenvalue λ_1 varies smoothly with temperature or other control parameters. This leads to the second essential result: Kato's analytic perturbation theorem [42].

Theorem 2. [Kato, adapted] *Let $\mathbf{V}(z)$ be a complex matrix whose entries are analytic functions of a parameter z . If $\lambda_1(z_0)$ is an isolated, simple eigenvalue, then there exists an analytic function $\lambda_1(z)$ defined near z_0 , such that both $\lambda_1(z)$ and its corresponding eigenvectors vary analytically with z .*

In physical applications, the parameter z often represents temperature T , but it may also correspond to other thermodynamic control variables such as magnetic field or chemical potential. If the transfer matrix $\mathbf{V}(z)$ depends analytically on z , and its dominant eigenvalue $\lambda_1(z)$ remains simple and isolated, then Kato's theorem [42] ensures that $\lambda_1(z)$ and its associated eigenvectors vary analytically with z . In particular, for $z = T > 0$, analyticity holds because Boltzmann weights are well-defined, and this smooth behavior of the dominant eigenvalue plays a central role in determining the thermodynamic properties of the system.

Combining these ideas leads to a rigorous conclusion about one-dimensional systems with short-range interactions, as formalized by Cuesta and Sánchez [3].

Theorem 3. [Non-existence of phase transitions in 1D systems] Let $\mathbf{V}(x, T)$ be a real, non-negative, irreducible matrix whose entries are analytic in both a control parameter x and temperature $T > 0$. Let $\lambda_1(x, T)$ denote its largest eigenvalue, assumed to be simple and isolated for all $T > 0$. Then the free energy per site,

$$f(x, T) = -T \ln \lambda_1(x, T), \quad (2)$$

is analytic in both x and T .

Here and throughout, we set Boltzmann's constant $k_B = 1$, so that $\beta = 1/T$ and temperature and inverse temperature may be used interchangeably.

Combining the analytic dependence of the transfer matrix $\mathbf{V}(x, T)$ with the simplicity and isolation of its dominant eigenvalue $\lambda_1(x, T)$, one obtains a rigorous constraint on the thermodynamic behavior of one-dimensional systems. The result, due to Cuesta and Sánchez [3], states that the free energy per site, defined in the thermodynamic limit by the leading eigenvalue, is an analytic function of both temperature and external parameters, provided $\mathbf{V}(x, T)$ remains irreducible and analytic. This analyticity rules out the possibility of genuine phase transitions, as no singularities can arise in $f(x, T)$ under these conditions.

2.2. Block-diagonal reducible matrices

To illustrate a scenario that permits non-analytic behavior, let us consider a transfer matrix \mathbf{V} that is reducible. For simplicity, assume \mathbf{V} decomposes into two decoupled irreducible submatrices \mathbf{A} and \mathbf{B} , such that

$$\mathbf{V} = \begin{pmatrix} \mathbf{A} & \mathbf{0} \\ \mathbf{0} & \mathbf{B} \end{pmatrix}. \quad (3)$$

Each block contributes its own dominant eigenvalue, denoted $w_a = \langle \phi_a | \mathbf{A} | \psi_a \rangle$ and $w_b = \langle \phi_b | \mathbf{B} | \psi_b \rangle$, with corresponding right (left) eigenvectors $|\psi_a\rangle$ ($\langle \phi_a|$) and $|\psi_b\rangle$ ($\langle \phi_b|$), respectively. According to the Perron-Frobenius theorem, both w_a and w_b are strictly positive and non-degenerate within their respective blocks.

The spectrum of \mathbf{V} is simply the union of the spectra of \mathbf{A} and \mathbf{B} . Hence, the two leading eigenvalues of \mathbf{V} are

$$\lambda_1 = \max(w_a, w_b), \quad (4)$$

$$\lambda_2 = \min(w_a, w_b). \quad (5)$$

Suppose now that \mathbf{V} depends on some external parameter x , such as a magnetic field or chemical potential. For a particular point (x_p, T_p) , the two leading eigenvalues may coincide, $w_a(x_p, T_p) = w_b(x_p, T_p)$, resulting in a true level crossing and a degeneracy in the spectrum. The corresponding free energy per site then becomes

$$f = -T \ln [\max(w_a, w_b)], \quad (6)$$

which is non-analytic at the crossing point (x_p, T_p) , signaling a first-order phase transition between decoupled sectors a and b .

At first glance, this seems to contradict the non-existence theorem discussed earlier. However, the key assumption of irreducibility is no longer satisfied: the decoupling of \mathbf{A} and \mathbf{B} violates the conditions of both the Perron-Frobenius and Cuesta-Sánchez theorems. The resulting non-analyticity is therefore consistent with the underlying theory.

This simple two-block decomposition captures the essential mechanism by which block-diagonal structure allows genuine thermodynamic singularities. In more complex cases with many disconnected sectors, the leading behavior is still often governed by the two most dominant blocks. Such effective two-block approximations are successfully applied in models like the Kittel model [43] and will be invoked again in the analysis of the nanowire model in Sec. 5.

2.3. Nearly block-diagonal irreducible matrices

Let us now consider a more subtle case: the transfer matrix \mathbf{V} is formally irreducible, but exhibits a nearly block-diagonal structure

$$\mathbf{V} = \begin{pmatrix} \mathbf{A} & \mathbf{C} \\ \mathbf{C}^T & \mathbf{B} \end{pmatrix}, \quad (7)$$

where \mathbf{A} and \mathbf{B} are dominant irreducible blocks and \mathbf{C} contains small off-diagonal couplings. Although \mathbf{V} is formally irreducible, the elements of \mathbf{C} may become suppressed at a given parameter value x_p , nearly decoupling the sectors \mathbf{A} and \mathbf{B} at a fixed temperature

To analyze the thermodynamics in this limit, we restrict \mathbf{V} to the subspace spanned by the leading eigenvectors $|\psi_a\rangle$, $|\psi_b\rangle$ of \mathbf{A} and \mathbf{B} , respectively. This yields the effective two-level matrix

$$\mathcal{V}_t = \begin{pmatrix} w_a & \langle \phi_a | \mathbf{C} | \psi_b \rangle \\ \langle \phi_b | \mathbf{C}^T | \psi_a \rangle & w_b \end{pmatrix}, \quad (8)$$

where $\langle \phi_a | \mathbf{C} | \psi_b \rangle > 0$ and $\langle \phi_b | \mathbf{C}^T | \psi_a \rangle > 0$, according to the condition of matrix non-negative and irreducibility, then let us define $\langle \phi_b | \mathbf{C}^T | \psi_a \rangle \langle \phi_a | \mathbf{C} | \psi_b \rangle = w_0^2$. Thus, the eigenvalues of \mathcal{V}_t are:

$$\lambda_{1,2} = \frac{1}{2} (w_a + w_b \pm \sqrt{(w_a - w_b)^2 + 4w_0^2}), \quad (9)$$

which exhibit an avoided crossing due to finite w_0 even when $w_a \approx w_b$. This guarantees analyticity of the free energy, despite the presence of a sharp thermodynamic crossover.

To make this structure more transparent, define the average eigenvalue $\bar{w} = \frac{1}{2}(w_a + w_b)$, and introduce the dimensionless spectral splitting:

$$\zeta = \frac{\sqrt{\sigma^2 + 4w_0^2}}{\bar{w}}, \quad (10)$$

with $\sigma = w_a - w_b$. The eigenvalues can then be rewritten as

$$\lambda_{1,2} = \bar{w} \left(1 \pm \frac{1}{2} \zeta \right). \quad (11)$$

We consider this case to show how weak inter-block couplings, though negligible at low temperatures, can lift degeneracies and induce avoided crossings between dominant eigenvalues at finite temperatures.

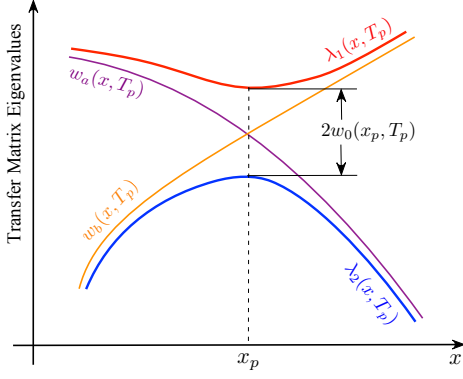


Figure 1: Schematic representation of the two leading eigenvalues λ_1 and λ_2 as a function of control parameter x at fixed temperature T_p . The minimal gap $2w_0$ appears at $x = x_p$, where $w_a = w_b$ when $w_0 \rightarrow 0$.

Thus, the free energy per site in the thermodynamic limit becomes analytic and is given by

$$f = -\frac{1}{\beta} \ln \left[\bar{w} \left(1 + \frac{1}{2} \zeta \right) \right]. \quad (12)$$

As $w_0 \rightarrow 0$, the ζ function (10) decreases and the spectral gap narrows, producing a sharp but analytic crossover. In this limit, the off-diagonal couplings vanish, and the pseudotransition sharpens toward an effective level crossing.

2.3.1. Avoided Crossing and Minimal Spectral Gap

To visualize the analytic structure discussed above, consider the behavior of the dominant eigenvalues $\lambda_1(x, T_p)$ and $\lambda_2(x, T_p)$ near the pseudo-critical point (x_p, T_p) . As illustrated in Fig. 1, these eigenvalues exhibit an avoided crossing: when the coupling $w_0 \rightarrow 0$, the weights w_a and w_b become degenerate at $x = x_p$, and the minimal gap between λ_1 and λ_2 closes asymptotically.

The leading-order condition for this crossover is given by the spectral balance $w_a(x_p, T_p) = w_b(x_p, T_p)$, which identifies the point (x_p, T_p) where the dominant sectors have equal statistical weight. This condition underlies many pseudotransition studies [12, 13, 14, 15, 24, 25, 26, 37] and will be revisited in Sec. 3.1.1 with explicit thermodynamic consequences.

The ζ function also can be approximate around the avoiding crossing through eigenvalue ratio:

$$\left(\frac{\lambda_2}{\lambda_1} \right) = \left(\frac{1 - \zeta/2}{1 + \zeta/2} \right) \approx e^{-\zeta}, \quad (13)$$

or, equivalently, eq.(10) can be more conveniently written as

$$\zeta = \ln \left(\frac{\lambda_1}{\lambda_2} \right). \quad (14)$$

This logarithmic form directly relates the spectral gap to the correlation length, which becomes $\xi = \zeta^{-1}$ in the absence of competing subdominant eigenvalues.

With the phenomenological context in place, we now turn to the central spectral analysis. Sec.3 introduces the general formalism of nearly reducible transfer matrices and their thermodynamic implications. This section forms the theoretical core

of the paper and will serve as the reference point for all model-specific analyses that follow.

3. Thermodynamic consequences of nearly block-diagonal structure

As discussed in Sec. 2.2, small off-diagonal elements in an otherwise block-structured transfer matrix prevent true level crossings and enforce analyticity. Nevertheless, when the dominant sectors are nearly degenerate, these weak couplings can generate sharp thermodynamic crossovers that closely resemble phase transitions. In this section, we examine the thermodynamic implications of this structure.

3.1. Expansion of the spectral gap and pseudo-critical point

To analyze the behavior of thermodynamic observables near a pseudotransition, we expand the normalized spectral gap $\zeta(x, T)$ in a Taylor series around the anomalous point (x_p, T_p) , as justified by Kato's theorem [42]. The full derivative expressions, including mixed and second-order terms, are derived in Appendix 7. Importantly, this expansion remains well-defined even when $w_a = w_b$, since the coupling $w_0 > 0$ ensures ζ stays analytic and nonzero. Expanding around the anomalous point (x_p, T_p) , we write:

$$\begin{aligned} \zeta(x, T) = & \zeta(x_p, T_p) + \zeta_{T_p} \delta T + \zeta_{x_p} \delta x + \\ & + \zeta_{T_p^2} \frac{\delta T^2}{2} + \zeta_{x_p^2} \frac{\delta x^2}{2} + \zeta_{x_p, T_p} \delta x \delta T \dots, \end{aligned} \quad (15)$$

where we are assuming $\delta T = T - T_p$ and $\delta x = x - x_p$. Derivatives such as $\zeta_T = \frac{\partial \zeta}{\partial T}$, and $\zeta_{T^2} = \frac{\partial^2 \zeta}{\partial T^2}$, are defined in the usual way. Similar definitions apply for derivatives with respect to x , and the mixed derivative is given by $\zeta_{x, T} = \frac{\partial^2 \zeta}{\partial x \partial T}$. The subscript p indicates that all derivatives are evaluated at the point (x_p, T_p) . Symbolically, the derivative of ζ with respect to a generic parameter (such as x or T) can be expressed in terms of \bar{w} , σ , and w_0 as follows

$$\zeta' = \frac{(\sigma \sigma' + 4w_0 w_0') \bar{w} - (\sigma^2 + 4w_0^2) \bar{w}'}{\bar{w}^2 \sqrt{\sigma^2 + 4w_0^2}}. \quad (16)$$

Here, the prime notation denotes the derivative with respect to a general parameter, either x or T , depending on the context. Fixing T_p , ζ attains a minimum at x_p if

$$\zeta_{x_p} = \left. \frac{\partial \zeta(x, T_p)}{\partial x} \right|_{x_p, T_p} = 0. \quad (17)$$

Similarly, we can evaluate the partial derivative ζ_T at the point (x_p, T_p) , yielding

$$\zeta_{T_p} = \left. \frac{\partial \zeta(x_p, T)}{\partial T} \right|_{x_p, T_p} \neq 0, \quad (18)$$

This condition characterizes a valley structure in the $x - T$ plane, where the depth or height of the valley is determined by

the value of $\zeta(x, T)$. In general, the minimum does not correspond to a well (i.e., a true critical point), which would require the gradient to vanish in both directions: $\nabla\zeta = (0, 0)$ at (x_p, T_p) . Instead, the valley indicates a sharp but analytic crossover consistent with a pseudotransition.

On the other hand, by fixing x_p , we can minimize ζ with respect to temperature. This yields the condition:

$$\zeta_{T_p^*} = \frac{\partial\zeta(x_p, T_p^*)}{\partial T} \Big|_{x_p, T_p^*} = 0, \quad (19)$$

for some temperature T_p^* . This defines the point where the spectral gap reaches its minimum along the temperature axis at fixed x_p .

Notably, when the difference $\Delta T = T_p - T_p^* \rightarrow 0$, the valley in the $x - T$ landscape becomes sharply localized, resembling a narrow canyon, as illustrated in Fig. 2. This geometric narrowing of the gap region reflects the robustness of the pseudotransition and marks the regime where thermodynamic quantities exhibit sharp but continuous changes.

3.1.1. Pseudo-critical temperature

In the regime where the off-diagonal coupling is small ($0 < w_0 \ll w_a \sim w_b$), the condition for the pseudo-critical temperature follows from the general minimum conditions for the spectral gap $\zeta(x, T)$, as derived in Appendix 7. In particular, Eq. (74) gives the temperature minimization of ζ , and Eq. (79) provides control parameter minimization. In the zeroth-order limit where excited-state contributions are negligible and $w_0 \rightarrow 0$, these lead directly to the simplified balance condition

$$w_a(x_p, T_p) = w_b(x_p, T_p), \quad (20)$$

discussed earlier. This expression captures the leading-order estimate for the pseudo-critical point where the statistical weights of the dominant sectors become equal. This is the well known condition explored in the literature when discussed the pseudo-critical temperature or ultra-narrow crossover point [12, 13, 14, 15, 24, 25, 26, 37].

A pseudotransition occurs when the dominant eigenvalues w_a and w_b of two weakly coupled sectors become nearly degenerate. Assuming the off-diagonal coupling w_0 is small, the pseudo-critical temperature T_p can be estimated using Eq. (20), derived in Appendix 7. Retaining only the ground and first excited states in each sector, one obtains:

$$e^{-\epsilon_p/T_p} = \frac{g_{b,0} + g_{b,1}e^{-\delta_{b,1}/T_p}}{g_{a,0} + g_{a,1}e^{-\delta_{a,1}/T_p}}, \quad (21)$$

where $g_{\alpha,0}$ ($g_{\alpha,1}$) denote the degeneracies of the ground (first excited) states in sector $\alpha \in \{a, b\}$, respectively. The quantity $\epsilon_p = \epsilon_{a,0}(x_p) - \epsilon_{b,0}(x_p)$ is the energy difference between the ground states, and $\delta_{a,1}(x_p)$, $\delta_{b,1}(x_p)$ are the excitation gaps within each sector. If excited states are negligible, this expression reduces to the simpler form

$$T_p = \frac{\epsilon_p}{\ln(g_{a,0}/g_{b,0})}, \quad (22)$$

which reproduces known results used in various studies of this anomalous behavior [12]. This confirms that the sharpness and position of the crossover are governed by both ground-state degeneracies and excitation structures. At T_p , the statistical weights of the two dominant sectors become comparable, resulting in a sharp but analytic thermodynamic crossover.

3.2. Interface residual entropy

At zero temperature, the entropy of a system reflects the macroscopic degeneracy of its ground state. When a control parameter x is tuned to a critical value x_c , the system may reach a phase boundary where two distinct ground-state configurations coexist. In such cases, both sectors, labeled a and b , contribute significantly to the partition function, giving rise to a finite entropy even at $T = 0$. This entropy, associated with the interface between competing ground states, is known as the critical residual entropy.

At finite temperature T_p where a pseudotransition occurs, the statistical weights of both sectors become comparable, leading to the condition

$$w_a = w_b \Rightarrow g_{a,0}e^{-(\bar{\epsilon}+\epsilon/2)/T_p} = g_{b,0}e^{-(\bar{\epsilon}-\epsilon/2)/T_p}, \quad (23)$$

where $\bar{\epsilon} = \frac{\epsilon_{a,0}(x) + \epsilon_{b,0}(x)}{2}$ and $\epsilon = \epsilon_{a,0}(x) - \epsilon_{b,0}(x)$.

Using the condition given by (22) we have $\frac{g_{a,0}}{g_{b,0}} = e^{\epsilon/T_p}$, which allows us to express the average weight as

$$\begin{aligned} \bar{w} &= \frac{1}{2} \left[g_{a,0}e^{-\epsilon/2T_p} + g_{b,0}e^{\epsilon/2T_p} \right] e^{-\bar{\epsilon}/T_p} \\ &= \sqrt{g_{a,0}g_{b,0}} e^{-\bar{\epsilon}/T_p}. \end{aligned} \quad (24)$$

The corresponding residual entropy at the phase boundary is then

$$\mathcal{S}_0^c = \ln \left(\sqrt{g_{a,0}g_{b,0}} \right). \quad (25)$$

At the critical point $x = x_c$, where the ground-state energies of the dominant sectors coincide, $\epsilon_{a,0}(x_c) = \epsilon_{b,0}(x_c) = \bar{\epsilon}_c$, this result reflects a situation in which both sectors contribute symmetrically to the thermodynamics.

This entropy corresponds to the geometric mean of the ground-state degeneracies and signals a dynamically balanced configuration, enforced by the pseudotransition condition of Eq. (22). It differs from a simple statistical mixture: the near-degeneracy and suppressed coupling lead to coherent coexistence rather than thermodynamic phase separation.

3.2.1. Residual entropy inequality

Assuming $g_{a,0} \geq g_{b,0}$, without loss of generality, we define the residual entropies of the adjacent pure sectors as $\mathcal{S}_0^a = \ln(g_{a,0})$, $\mathcal{S}_0^b = \ln(g_{b,0})$. The interface residual entropy derived in Eq. (25), results in $\mathcal{S}_0^c = \frac{1}{2}(\mathcal{S}_0^a + \mathcal{S}_0^b)$, then satisfies the inequality

$$\mathcal{S}_0^b \leq \mathcal{S}_0^c \leq \mathcal{S}_0^a, \quad (26)$$

which expresses that the crossover entropy lies between those of the competing sectors. This is a direct consequence of the nearly block-diagonal matrix structure and the balancing condition at the pseudotransition. Violating this inequality precludes

a pseudotransition, although satisfying it alone is not sufficient. This provides a relaxed version of the criterion previously discussed in Ref. [21].

The entropy (26) inequality offers a useful diagnostic tool: it characterizes pseudotransition-like behavior in systems with finite-range interactions, while preserving analyticity of the free energy. It emerges naturally from the weak coupling between dominant irreducible sectors in a nearly block-diagonal transfer matrix.

The interface residual entropy \mathcal{S}_0^c measures the configurational complexity at the crossover. When $\mathcal{S}_0^c \in [\mathcal{S}_0^b, \mathcal{S}_0^a]$, the sectors contribute comparably, allowing a pseudotransition. In contrast, models with interface frustration, or symmetry mixing often yield $\mathcal{S}_0^c > \max(\mathcal{S}_0^a, \mathcal{S}_0^b)$, signaling excess disorder at the interface and forbidding a pseudotransition.

4. Doniach one-dimensional model

To illustrate the proposed formalism, we consider a representative model that captures the essential features of pseudotransitions in one-dimensional systems. Specifically, we study an Ising chain with internal degeneracy, where one spin state carries a macroscopic multiplicity. In particular, it shares structural features with the model proposed by Doniach[40] to describe lipid chain ordering in biomembranes[44]. While our focus here is on the spectral and thermodynamic aspects of degeneracy-induced pseudotransitions, this biological motivation reinforces the broader relevance of such models. Despite its simplicity, this model is relevant to physical systems such as biomembranes, hydrogen-bonded chains, and DNA denaturation (for detail see Section 4.2 of Ref. [27]), and it exhibits pseudo-critical behavior closely related to that seen in Potts-like and Zimm-Bragg-type models [25, 45]. Furthermore, several more elaborated models can be mapped to similar effective forms via decoration transformations [46], making this a useful minimal prototype for analyzing pseudotransitions.

4.1. Hamiltonian and transfer matrix

In Doniach's original model [40], the system is a one-dimensional chain of variables $s_i = \pm 1$, representing two conformational states of a lipid chain e.g., $s_i = +1$ for the ordered (a) state and $s_i = -1$ for the disordered (b) state. The simplified Hamiltonian is

$$\mathcal{H} = -J \sum_i s_i s_{i+1} - h_{\text{eff}}(T) \sum_i s_i, \quad (27)$$

where $J > 0$ favors alignment (e.g., adjacent a -states), and $h_{\text{eff}}(T)$ is a temperature-dependent effective field that represents entropic and energetic contributions. Specifically, $h_{\text{eff}}(T) = \frac{1}{2}(E_s + \pi\Delta A + zW - T\mathcal{S}_{\text{eff}})$, with E_s the excitation energy from state a to b , $\pi\Delta A$ the mechanical work due to area expansion, zW the interchain interaction energy, and $\mathcal{S}_{\text{eff}} = k_B \ln(m_{\text{eff}})$ the configurational entropy of the b -state.

Now we can interpret as internal degeneracy, the state $s_i = -1$ has multiplicity $m_{\text{eff}} \geq 1$, while $s_i = +1$ remains non-degenerate. Although this modification does not alter the energy spectrum, it modifies the statistical weights in the parti-

tion function by introducing a degeneracy factor associated with each occurrence of $s_i = -1$.

An effective way to represent this asymmetry is by redefining the Hamiltonian to include an entropic term:

$$\mathcal{H}_{\text{eff}} = -J \sum_{i=1}^N s_i s_{i+1} - \sum_{i=1}^N \left[h s_i + (1 - s_i) \frac{\ln(m_{\text{eff}})}{2\beta} \right], \quad (28)$$

where $\beta = 1/T$ and Boltzmann's constant is set to unity. This form shifts the energy associated with the $s_i = 1$ state by a temperature-dependent term, effectively encoding the degeneracy m_{eff} through a modified Boltzmann factor.

The resulting 2×2 transfer matrix becomes

$$\mathbf{V} = \begin{pmatrix} e^{\beta(J+h)} & m_{\text{eff}} e^{-\beta(J-h)} \\ e^{-\beta(J+h)} & m_{\text{eff}} e^{\beta(J-h)} \end{pmatrix}, \quad (29)$$

where the matrix elements correspond to the Boltzmann weights of neighboring spin pairs (s_i, s_{i+1}) . The degeneracy m_{eff} modifies the statistical weight of configurations involving the -1 state, introducing entropic competition between sectors.

This simple modification captures key features relevant to pseudotransition behavior and allows full analytical treatment, making it a suitable minimal model for illustrating the general framework.

According to Sec. 2.2, we can interpret the corresponding block-diagonal matrix, which in this case consists of the diagonal elements of Eq. (29), with associated dominant configurations $|\psi_a\rangle = |+\rangle$ and $|\psi_b\rangle = |-\rangle$, and corresponding weights $w_a = e^{\beta(J+h)}$ and $w_b = m_{\text{eff}} e^{\beta(J-h)}$, respectively. Evidently, the off-diagonal elements of matrix \mathbf{V} become negligible in the limit $\beta \rightarrow \infty$ and $J > 0$. In this regime, the system undergoes a zero-temperature phase transition between the fully spin-down state $|\psi_b\rangle$ and the fully spin-up state $|\psi_a\rangle$. Note that spin-inversion symmetry holds only when $m_{\text{eff}} = 1$.

4.2. Pseudo-critical temperature and interface residual entropy

To analyze the thermodynamic behavior near the pseudotransition, we use the framework developed in Sec. 2.3. Identifying the dominant weights as $w_a = e^{\beta(J+h)}$, $w_b = m_{\text{eff}} e^{\beta(J-h)}$, and $w_0 = \sqrt{m_{\text{eff}}} e^{-\beta J}$, the spectral structure is governed by

$$\bar{w} = \frac{e^{\beta J}}{2} (e^{\beta h} + m_{\text{eff}} e^{-\beta h}), \quad \sigma = e^{\beta J} (e^{\beta h} - m_{\text{eff}} e^{-\beta h}), \quad (30)$$

and the spectral gap (10), becomes

$$\zeta = \frac{\sqrt{\sigma^2 + 4m_{\text{eff}} e^{-2\beta J}}}{\bar{w}}. \quad (31)$$

Recall from Sec. 2.3 that ζ also controls the thermodynamic signatures, and small ζ enhances the pseudotransition.

To determine the pseudo-critical temperature, we apply the condition $\partial_h \zeta = 0$, as given by Eq. (79). This condition reduces to $w_a = w_b$, which leads to the closed-form expression:

$$T_p = \frac{2h_p}{\ln(m_{\text{eff}})}, \quad (32)$$

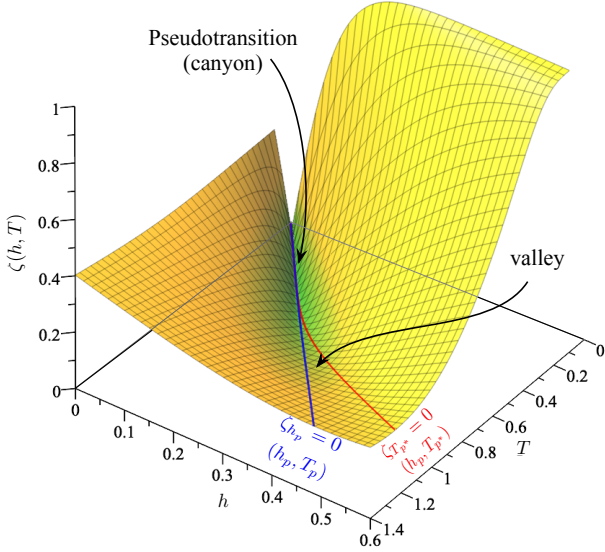


Figure 2: Surface plot of $\zeta(h, T)$ in the $h - T$ plane for $m_{\text{eff}} = 2$ and $J = 1$. The blue curve corresponds to the condition $\zeta_h = 0$ [(32)], while the red curve follows $\zeta_T = 0$ [(34)].

consistent with previous results[27].

We may also compute the value T_{p^*} that minimizes ζ with respect to temperature, i.e., using $\zeta_{T_{p^*}} = 0$ from Eq.(74). The result reads

$$(m_{\text{eff}} - e^{2\beta h})he^{4\beta J} + (2J + h)e^{2\beta h} + (2J - h)m_{\text{eff}} = 0, \quad (33)$$

which, to leading order in the low-temperature regime, becomes:

$$e^{2\beta h_p} = m_{\text{eff}} \frac{e^{4\beta J} - 1 + 2J/h_p}{e^{4\beta J} - 1 - 2J/h_p}, \quad (34)$$

$$e^{2\beta h_p} \approx m_{\text{eff}} + \frac{4J\omega}{h_p} e^{-4\beta J}. \quad (35)$$

yielding the approximate correction, in analogy a (32), we have

$$T_{p^*} \approx \frac{2h_p}{\ln(m_{\text{eff}}) + \frac{4J}{h_p} e^{-4J/T_{p^*}}}. \quad (36)$$

Since $J > 0$ and $\beta \gg 1$, the correction term in Eq. (35) becomes negligible, and T_p and T_{p^*} are of the same leading order.

Fig. 2 shows the surface $\zeta(h, T)$ for fixed parameters $m_{\text{eff}} = 2$ and $J = 1$. The blue curve corresponds to $\zeta_h = 0$ [see (32)] and the red curve to $\zeta_T = 0$ [see (34)]. At higher temperatures, these curves are well separated, but as temperature decreases, they converge near a characteristic field h_p . This convergence defines a narrowing valley in the (h, T) -plane, resembling a ‘‘spectral canyon’’, with a floor given by the minimal values of ζ . As $T \rightarrow 0$, the gap region becomes increasingly localized, signaling the sharpening of the pseudotransition. Although the free energy remains analytic throughout, this spectral structure reflects strong competition between sectors and underpins the rapid thermodynamic crossover characteristic of pseudotransitions.

At this point, the Boltzmann weights of the competing spin sectors become equal. For this model, the corresponding residual entropy is $S_0^c = \frac{1}{2} \ln(m_{\text{eff}}) = \frac{1}{2} S_{\text{eff}}$, which follows directly

from (25), in agreement with the result reported in Ref. [27]. This residual entropy satisfies the inequality given in Eq. (26),

$$0 < S_0^c = \frac{1}{2} S_{\text{eff}} < S_{\text{eff}}, \quad (37)$$

consistent with the general criterion discussed in Sec.3.2.1. It reflects the partial contribution of degenerate configurations at the crossover and confirms the presence of a pseudotransition, characterized by near-degenerate dominant eigenvalues and a nearly block-diagonal transfer matrix structure.

Surely, this approach can also be applied to higher spins, as explored in Ref. [27] for spin-1 systems, which involve a cubic-root equation.

5. Mixed spin-1/2 and spin-1 hexagonal nanowire system

The next model we consider contrasts with the previous one. Here, our goal is to demonstrate how a high-dimensional transfer matrix can be systematically reduced, first using symmetries, and then through the nearly block-diagonal structure central to pseudotransition behavior.

In this context, motivated by experimental results, several studies have investigated magnetic nanowire systems with core-shell architectures, revealing distinctive behaviors in different materials. For example, single-crystal Co_3O_4 nanowires exhibit two Néel temperatures (56 K and 73 K) due to magnetic proximity effects between core and shell regions[47]; large-scale Co-Zn-P nanowire arrays synthesized via electroless deposition show characteristic magnetic responses linked to their composition and structure[48]; and Co-Cu nanowire arrays created using galvanic displacement deposition demonstrate tunable microstructures and magnetic properties[49]. Several related theoretical investigations have been carried out, such as the one developed in Ref. [50, 51]. Therefore, we analyze the mixed-spin hexagonal nanowire model studied in Refs. [38, 52], consisting of an Ising spin-1/2 (red circles) coupled to spin-1 Blume-Capel variables (blue circles), as illustrated in Fig.3.

The system is defined on a cylindrical geometry and described by the Hamiltonian $\mathcal{H} = \sum_{i=1}^N H_{i,i+1}$, with

$$H_{i,i+1} = - \sum_{j=1}^6 \left[J_s (S_{j,i} S_{j,i+1} + S_{j,i} S_{j+1,i}) + J_1 S_{j,i} \sigma_i + J_c \sigma_i \sigma_{i+1} + D S_{j,i}^2 \right], \quad (38)$$

where $\sigma_i \in \{-\frac{1}{2}, \frac{1}{2}\}$ denotes the spin-1/2 core spin and $S_{j,i} \in \{-1, 0, 1\}$ the spin-1 shell spin at position j in the i -th hexagonal unit. We assume periodic boundary conditions. The coupling constants are: J_1 between Ising and Blume-Capel spins, J_c between core Ising spins, and J_s between neighboring shell spins; D is the single-ion anisotropy (crystal field).

5.0.1. Ferromagnetic (FM) phase

For $D > -2.5$, the ground state of the system is ferromagnetic (FM), with both core and shell spins fully aligned. The

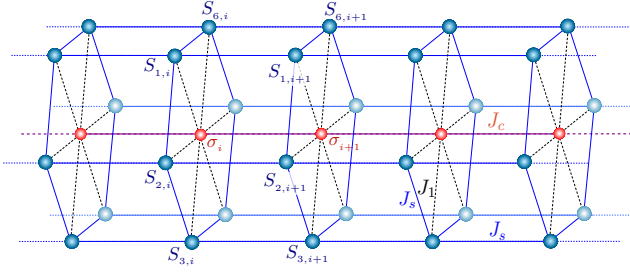


Figure 3: Schematic representation of mixed spin-1/2 (red) and spin-1 (blue) hexagonal nanowire. Shell spins interact via J_s , core-shell via J_1 , and core-core via J_c .

corresponding ground-state energy per unit cell is

$$E_{FM} = -\frac{61}{4} - 6D. \quad (39)$$

Each unit cell configuration is denoted by

$$|a_\tau^{(0)}\rangle = |\tau, \tau, \tau, \tau, \tau, \tau\rangle \otimes |\frac{\tau}{2}\rangle,$$

where $\tau = \pm 1$. The first ket corresponds to the shell spin-1 states, while the second ket denotes the core spin-1/2 state. The full ground state is the symmetric superposition over all N unit cells:

$$|FM\rangle = 2^{-N/2} \bigotimes_{i=1}^N (|a_+^{(0)}\rangle_i + |a_-^{(0)}\rangle_i). \quad (40)$$

This state is doubly degenerate due to global spin-inversion symmetry. Although each configuration is magnetically ordered, the overall thermal average of the magnetization vanishes: $m_c = m_s = 0$.

5.0.2. Core-ferromagnetic (CFM) phase

For $D < -2.5$, the ground state shifts to a core-ferromagnetic (CFM) configuration, where the core spins are aligned while the shell spins are fully suppressed into the $S = 0$ state. The corresponding ground-state energy per unit cell is

$$E_{CFM} = -\frac{1}{4}. \quad (41)$$

Each unit cell state is given by

$$|b_\tau^{(0)}\rangle = |0, 0, 0, 0, 0\rangle \otimes |\frac{\tau}{2}\rangle,$$

where $\tau = \pm 1$. The full ground state takes the form

$$|CFM\rangle = 2^{-N/2} \bigotimes_{i=1}^N (|b_+^{(0)}\rangle_i + |b_-^{(0)}\rangle_i), \quad (42)$$

This state is also doubly degenerate due to global spin inversion. Since the shell spins are in non-magnetic $S = 0$ states, we have $m_s = 0$, and the net core-spin magnetization averages to zero: $m_c = 0$.

5.1. Reducible block transfer matrix

We now apply the transfer matrix method to compute the free energy of the nanowire model defined by the Hamiltonian in Eq. (38). The full transfer matrix \mathbf{V} has dimension 1458×1458 , with elements defined as

$$\langle \sigma, \{S_i\} | \mathbf{V} | \{S'_i\}, \sigma' \rangle = e^{-H_{i,i+1}/k_B T}, \quad (43)$$

where $\{S_i\} = \{S_1, S_2, S_3, S_4, S_5, S_6\}$ denotes the spin-1 shell configuration of the hexagon at site i , and $\sigma \in \{-\frac{1}{2}, \frac{1}{2}\}$ is the core spin.

This transfer matrix is reducible due to the geometric and spin symmetries of the system. In particular, the hexagonal symmetry group C_6 acts by cyclic permutation:

$$C_6 |S_1, S_2, S_3, S_4, S_5, S_6\rangle = |S_2, S_3, S_4, S_5, S_6, S_1\rangle, \quad (44)$$

with the full group given by $C_6 \mapsto \{I, C_6, C_6^2, \dots, C_6^5\}$. In addition, the system is invariant under spatial reflection \mathcal{R} through the center of the hexagon:

$$\mathcal{R} |S_1, S_2, S_3, S_4, S_5, S_6\rangle = |S_6, S_5, S_4, S_3, S_2, S_1\rangle, \quad (45)$$

with $\mathcal{R} \mapsto \{I, \mathcal{R}\}$.

Taking into account the full C_6 symmetry, the transfer matrix decomposes into a direct sum of irreducible subspaces. The shell space of dimension $3^6 = 729$ can be block-diagonalized under these symmetries, and the full transfer matrix \mathbf{V} of dimension $1458 = 2 \times 729$ can be reduced accordingly.

This symmetry reduction leads to the decomposition:

$$3^6 \otimes 2 = 184 \oplus 178 \oplus 172 \oplus 3(\oplus 160) \oplus 6(\oplus 74), \quad (46)$$

where $n(\oplus d)$ denotes n blocks of dimension d . Moreover, in the absence of external fields, the model is symmetric under global spin inversion (\mathbb{Z}_2), $(S_j^z, \sigma^z) \mapsto (-S_j^z, -\sigma^z)$, which allows further reduction of \mathbf{V} into even and odd parity sectors of dimension 729×729 .

Each of these sectors further decomposes as:

$$3^6 = 92 \oplus 89 \oplus 86 \oplus 3(\oplus 80) \oplus 6(\oplus 37). \quad (47)$$

The dominant eigenvalue, which governs the free energy in the thermodynamic limit, lies in the largest irreducible block of size 92×92 , associated with the fully symmetric subspace under rotations, reflections, and global spin inversion. As shown in Ref. [38], this eigenvalue is non-degenerate and satisfies the Perron-Frobenius theorem, ensuring analyticity and excluding a true phase transition.

5.2. Nearly block-diagonal matrix

The mean-field approximation (MFA) [52] indicates a first-order phase transition at finite temperature near $D = -2.5$, for coupling constants $J_1 = J_s = J_c = 1$. However, a subsequent analysis using the numerical transfer matrix method [38] revealed that the system exhibits only a pseudotransition, with no genuine thermodynamic singularity.

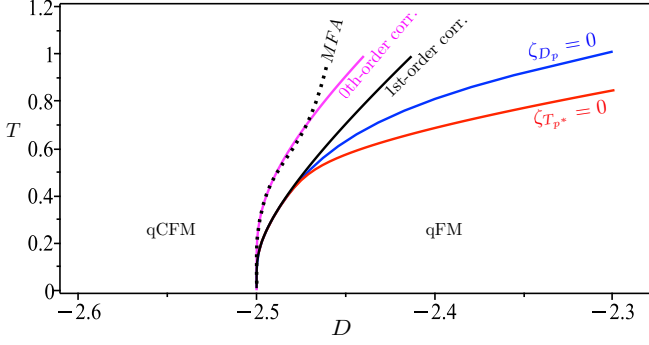


Figure 4: Pseudo-critical temperature T_p as a function of D , assuming zero magnetic field and fixed $J_1 = J_s = J_c = 1$. The curves correspond to different pseudotransition conditions: (74) (blue curve), (79) (red curve), the 0th-order correction (49) (pink curve), and 1st-order correction (65) (black curve). The dashed line shows the MFA result from [52].

5.2.1. 0th-order correction

At zeroth order, we neglect all low-lying excited states and retain only the dominant ground-state configurations $\{|a^{(0)}\rangle, |b^{(0)}\rangle\}$, corresponding to the FM and CFM sectors, respectively. In this approximation, the transfer matrix reduces to a 2×2 effective form:

$$\mathbf{V}_t^{(0)} = \begin{pmatrix} x^{12} (y^{61} \pm y^{11}) & y^{17} x^6 (y^2 \pm 1) \\ y^{17} x^6 (y^2 \pm 1) & \frac{y^2 \pm 1}{y} \end{pmatrix}, \quad (48)$$

with $y = e^{J_c/4T}$ and $x = e^{D/2T}$. The (+) sign corresponds to the symmetric sector, and the (-) sign to the antisymmetric one.

As discussed in Sec. 2.3, $\zeta = \ln(\lambda_1^{(0)}/\lambda_2^{(0)})$ reaches a minimum at the pseudo-critical point, providing a local diagnostic for anomalous thermodynamics.

Comparing matrix (48) with the general effective matrix form given in Eq. (8), and applying the pseudo-critical condition (20) $w_a = w_b$, we obtain the following transcendental equation from the diagonal elements of the symmetric block:

$$e^{-\frac{2D_p + J_c}{4T_p}} \left(e^{\frac{25J_c}{2T_p}} + 1 \right) = \left(e^{\frac{J_c}{2T_p}} + 1 \right). \quad (49)$$

Solving this equation numerically for fixed $J_c = 1$, we obtain the pseudo-critical temperature $T_p(D)$, plotted as the pink curve in Fig. 4. Surprisingly, this analytical result matches well with the MFA prediction (dashed line) from Ref. [52], which was originally interpreted as signaling a first-order phase transition.

5.2.2. 1st-order correction

In the low-temperature regime, the system is primarily governed by ground-state configurations. However, as temperature increases, thermal fluctuations begin to populate low-lying excited states. For simplicity, we label the dominant sectors as regions a and b , following the conventions introduced in Sec. 2.2.

The first excited states within each region can be defined using the following symmetric combinations. For region a , we define:

$$|a_\tau^{(1)}\rangle = \frac{1}{\sqrt{6}} (|\tau\tau\tau\tau\tau 0\rangle + \sqrt{5} |\tau\tau\tau 0\tau 0\rangle) \otimes |\frac{\tau}{2}\rangle, \quad (50)$$

which represents the leading fluctuation above the FM ground state. Similarly, for region b , we denote

$$|b_\tau^{(1)}\rangle = \frac{1}{\sqrt{6}} (|00000\tau\rangle + \sqrt{5} |000\tau 0\tau\rangle) \otimes |\frac{\tau}{2}\rangle, \quad (51)$$

corresponding to the dominant fluctuation above the CFM ground state.

To construct the truncated transfer matrix, we apply spin-inversion symmetry to build the parity-even combinations

$$|a^{(k)}\rangle = \frac{1}{\sqrt{2}} (|a_+^{(k)}\rangle + |a_-^{(k)}\rangle), \quad (52)$$

$$|b^{(k)}\rangle = \frac{1}{\sqrt{2}} (|b_+^{(k)}\rangle + |b_-^{(k)}\rangle), \quad (53)$$

with $k = 0, 1$. Using the truncated basis $\{|a^{(0)}\rangle, |a^{(1)}\rangle, |b^{(0)}\rangle, |b^{(1)}\rangle\}$, the irreducible transfer matrix becomes

$$\mathbf{V}_t^{(1)} = \begin{pmatrix} v_{1,1} & v_{1,2} & v_{1,3} & v_{1,4} \\ v_{1,2} & v_{2,2} & v_{2,3} & v_{2,4} \\ v_{1,3} & v_{2,3} & v_{3,3} & v_{3,4} \\ v_{1,4} & v_{2,4} & v_{3,4} & v_{4,4} \end{pmatrix}, \quad (54)$$

with matrix elements given by

$$\begin{aligned} v_{1,1} &= x^{12} (y^{61} \pm y^{11}), \\ v_{1,2} &= y^{10} x^{11} (y^{42} \pm 1) \sqrt{6}, \\ v_{1,3} &= y^{14} x^7 (y^{10} \pm 1) \sqrt{6}, \\ v_{1,4} &= y^{17} x^6 (y^2 \pm 1), \\ v_{2,2} &= x^{10} y^5 (y^{42} 5y^{38} \pm 5y^4 \pm 1), \\ v_{2,3} &= x^6 y^9 (5y^{10} + y^6 \pm y^4 \pm 5), \\ v_{2,4} &= y^{12} x^5 (y^2 \pm 1) \sqrt{6}, \\ v_{3,3} &= \frac{x^2 (y^{10} + 5y^6 \pm 5y^4 \pm 1)}{y^3}, \\ v_{3,4} &= x (y^2 \pm 1) \sqrt{6}, \\ v_{4,4} &= \frac{y^2 \pm 1}{y}, \end{aligned} \quad (55)$$

with $y = e^{J_c/4T}$ and $x = e^{D/2T}$. The (+) sign corresponds to the symmetric sector and the (-) sign to the antisymmetric one.

We now rewrite the truncated transfer matrix $\mathbf{V}_t^{(1)}$ in block form, separating regions a and b as:

$$\mathbf{V}_t^{(1)} = \begin{pmatrix} \mathbf{A} & \mathbf{C} \\ \mathbf{C}^T & \mathbf{B} \end{pmatrix}, \quad (56)$$

where

$$\mathbf{A} = \begin{pmatrix} v_{1,1} & v_{1,2} \\ v_{1,2} & v_{2,2} \end{pmatrix}, \quad \mathbf{B} = \begin{pmatrix} v_{3,3} & v_{3,4} \\ v_{3,4} & v_{4,4} \end{pmatrix}, \quad \mathbf{C} = \begin{pmatrix} v_{1,3} & v_{1,4} \\ v_{2,3} & v_{2,4} \end{pmatrix}.$$

If off-diagonal block \mathbf{C} is sufficiently small in the regime of interest, we can neglect its contribution and approximate $\mathbf{V}_t^{(1)}$ as block-diagonal. In this limit, the eigenvalues and eigenstates can be obtained independently for each sector.

Sector a (quasi-ferromagnetic):. Diagonalizing \mathbf{A} , the symmetric eigenvalue is given by

$$w_a = \frac{v_{1,1} + v_{2,2} + \sqrt{(v_{1,1} - v_{2,2})^2 + 4v_{1,2}^2}}{2}, \quad (57)$$

with corresponding eigenstate

$$|\psi_a\rangle = \sin(\theta_a)|a^{(0)}\rangle + \cos(\theta_a)|a^{(1)}\rangle, \quad (58)$$

where $\tan(2\theta_a) = \frac{2v_{1,2}}{v_{1,1} - v_{2,2}}$. The state $|\psi_a\rangle$ is a coherent mixture of the four configurations $\{|a_{\pm}^{(0)}\rangle, |a_{\pm}^{(1)}\rangle\}$, and defines the quasi-ferromagnetic (qFM) collective state:

$$|qFM\rangle = \bigotimes_{i=1}^N |\psi_a\rangle_i. \quad (59)$$

At low temperatures, $|\psi_a\rangle$ is dominated by the ground state $|a\tau^{(0)}\rangle$, with small thermal admixture from $|a\tau^{(1)}\rangle$. Since θ_a depends on temperature, the qFM state evolves with thermal fluctuations.

Sector b (quasi-core-ferromagnetic):. Similarly, diagonalizing \mathbf{B} , we obtain the symmetric eigenvalue

$$w_b = \frac{v_{3,3} + v_{4,4} + \sqrt{(v_{3,3} - v_{4,4})^2 + 4v_{3,4}^2}}{2}, \quad (60)$$

with eigenstate

$$|\psi_b\rangle = \sin(\theta_b)|b^{(0)}\rangle + \cos(\theta_b)|b^{(1)}\rangle, \quad (61)$$

with $\tan(2\theta_b) = \frac{2v_{3,4}}{v_{3,3} - v_{4,4}}$. The state $|\psi_b\rangle$ is a mixture of states $\{|b_{\pm}^{(0)}\rangle, |b_{\pm}^{(1)}\rangle\}$, and defines the quasi-core-ferromagnetic (qCFM) state as

$$|qCFM\rangle = \bigotimes_{i=1}^N |\psi_b\rangle_i. \quad (62)$$

As with qFM, the qCFM state incorporates temperature-dependent fluctuations through $\theta_b(T)$. Both qFM and qCFM reflect entropically dressed ground states that become relevant as temperature increases, and together they define the thermodynamic sectors responsible for the pseudotransition.

Effective transfer matrix:. Using the truncated matrix approach, we can estimate the largest eigenvalues of the nanowire model near the anomalous region with good accuracy. To do so, we construct an effective 2×2 irreducible matrix in the basis $\{|\psi_a\rangle, |\psi_b\rangle\}$, now including off-diagonal coupling terms, as introduced in Sec. 2.2. The resulting effective transfer matrix reads:

$$\mathcal{V}^{(1)} = \begin{pmatrix} w_a & \langle\psi_a|\mathbf{C}|\psi_b\rangle \\ \langle\psi_b|\mathbf{C}^T|\psi_a\rangle & w_b \end{pmatrix}. \quad (63)$$

The corresponding dominant eigenvalues of the transfer matrix are

$$\lambda_{1,2}^{(1)} = \frac{1}{2}(w_a + w_b \pm \sqrt{(w_a - w_b)^2 + 4w_0^2}), \quad (64)$$

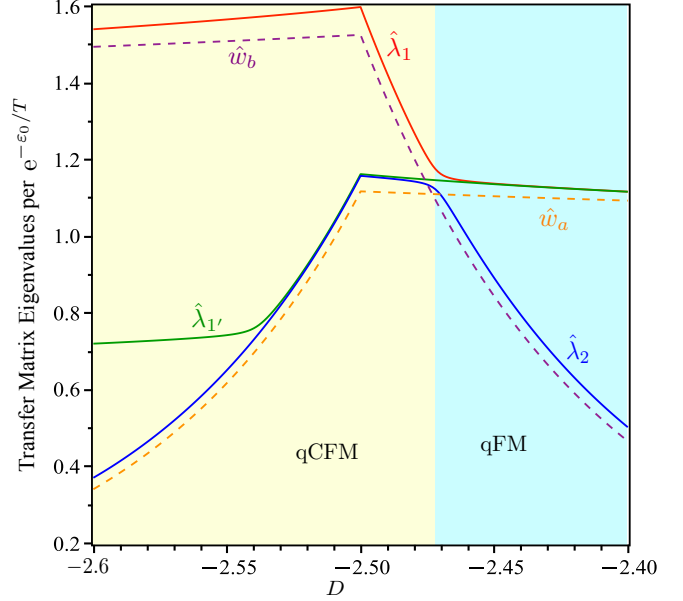


Figure 5: Leading eigenvalues of the transfer matrix as a function of D at fixed temperature $T = 0.5$. Solid curves represent exact numerical results: the red curve shows $\hat{\lambda}_1$, the blue curve shows $\hat{\lambda}_2$, and the orange curve corresponds to $\hat{\lambda}_1'$. Dashed lines indicate the first-order approximations \hat{w}_a and \hat{w}_b from the truncated matrix analysis.

where the off-diagonal overlap is defined by $\langle\psi_a|\mathbf{C}|\psi_b\rangle\langle\psi_b|\mathbf{C}^T|\psi_a\rangle = w_0^2$.

To determine the pseudo-critical temperature, we impose the condition $w_a = w_b$, analogous to Eq. (20). Using the explicit eigenvalue expressions from the symmetric blocks \mathbf{A} and \mathbf{B} , this yields the transcendental equation

$$\frac{v_{1,1} + v_{2,2} + \sqrt{(v_{1,1} - v_{2,2})^2 + 4v_{1,2}^2}}{v_{3,3} + v_{4,4} + \sqrt{(v_{3,3} - v_{4,4})^2 + 4v_{3,4}^2}} = 1. \quad (65)$$

where all matrix elements $v_{i,j}$ are defined in Eq. (55) (with the (+) sign). Solving this equation yields the pseudo-critical temperature T_p as a function of D .

The first-order correction result is shown in Fig. 4 as the black solid curve. It differs notably from the zeroth-order approximation (pink curve) and the MFA prediction, although all three converge in the low-temperature limit $T \rightarrow 0$. The same figure also displays two exact conditions: the blue curve corresponds to $\zeta_{T_p^*} = 0$, obtained from Eq. (74), and the red curve corresponds to $\zeta_{D_p} = 0$, derived from Eq. (79).

For temperatures $T \lesssim 0.5$, we observe that $T_p - T_p^* \rightarrow 0$, and the blue and red curves nearly coincide, forming a deep canyon-like structure, as seen in Fig. 4. As temperature increases, the curves gradually diverge, outlining a valley. Notably, our first-order approximation tracks both minimized curves closely across the entire range, confirming that the first-order effective matrix yields an accurate estimate of the pseudo-critical temperature $T_p(D)$ throughout the anomalous region.

To assess the accuracy of the truncated effective matrix with first-order corrections, we compare its predictions to the exact leading eigenvalues of the full transfer matrix. Fig. 5 shows the

normalized eigenvalues $\hat{\lambda}_i = \lambda_i e^{\varepsilon_0/T}$, where $\varepsilon_0 = \min(-\frac{1}{4}, -\frac{61}{4} - 6D)$ is the ground-state energy used to regularize the scale. For reference, we also include the first-order approximations $\hat{w}_a = w_a e^{\varepsilon_0/T}$ and $\hat{w}_b = w_b e^{\varepsilon_0/T}$ obtained from the reduced 4×4 matrix defined in Sec. 5.2.2.

Fig.5 illustrates the leading eigenvalues $\hat{\lambda}_1$ (solid red curve) and $\hat{\lambda}_2$ (solid blue curve), corresponding to the exact numerical eigenvalues computed from the full 92×92 symmetry-reduced transfer matrix. An avoided crossing is observed near the pseudo-critical value of D . The green curve represents $\hat{\lambda}_{1'}$, the largest eigenvalue of the 92×92 antisymmetric sector of the transfer matrix, which corresponds to the second-largest eigenvalue of the full system. This sector is obtained through symmetry reduction alone, without any truncation or approximation.

Interestingly, $\hat{\lambda}_{1'}$ remains nearly flat in the vicinity of the pseudotransition and is largely insensitive to variations in D . Despite being the second-largest eigenvalue in magnitude, its thermodynamic contribution is suppressed because it originates from a sector orthogonal to the dominant symmetric eigenstates. This highlights that $\hat{\lambda}_2$, not $\hat{\lambda}_{1'}$, governs the crossover with $\hat{\lambda}_1$, and confirms that the first-order approximation accurately captures the structure and evolution of the relevant eigenstates near the anomalous region. For additional detail see Ref. [38].

Residual entropy inequality: Finally, we verify the residual entropy inequality condition. Since both the FM and CFM phases are non-macroscopically degenerate, we have $g_a = g_b = 1$, which implies $S_a = S_b = 0$. Consequently, the interface residual entropy (25) becomes $S_0^c = \ln(\sqrt{g_a g_b}) = 0$, and the inequality (26) is exactly satisfied

$$S_0^b = S_0^c = S_0^a = 0. \quad (66)$$

There is no entropic competition between sectors, and the interface behaves thermodynamically like the surrounding phases. In contrast to models where interface frustration leads to $S_0^c > \max(S_0^a, S_0^b)$, here the residual entropy remains zero throughout.

6. Conclusion

This work establishes a unifying mechanism for pseudotransitions in one-dimensional systems: they emerge from irreducible but nearly block-diagonal transfer matrices. In the low temperature region, off-diagonal elements coupling distinct symmetry sectors become exponentially suppressed due to high excitation energies. Although these elements remain nonzero, ensuring strict irreducibility as required by the Perron-Frobenius theorem, their small magnitude makes the matrix behave as effectively reducible over finite temperature ranges. We define this regime as nearly block-diagonal irreducibility, in which the spectral and thermodynamic behavior closely resembles that of a reducible system, despite the absence of genuine singularities.

The key insight is that irreducibility suppresses nonanalyticities, preventing true phase transitions by forbidding eigenvalue crossings. Yet, when the dominant eigenvalues from weakly

coupled sectors approach each other, sharp but analytic thermodynamic crossovers arise. This pseudotransition reflects avoided crossings driven by low-temperature spectral competition, not actual symmetry breaking. Phase transitions occur only when irreducibility is lost, i.e., when inter-sector couplings vanish, allowing disconnected matrix blocks and exact level crossings.

To formalize this, we analyzed the spectral gap function $\zeta(x, T) = \ln(\lambda_1/\lambda_2)$ and derived general pseudo-critical conditions based on its extrema. This condition emerges from eigenvalue competition between leading symmetry-reduced sectors whose coupling is too weak to induce mixing but sufficient to lift degeneracies. The mechanism was demonstrated in two models. In the Ising chain with internal degeneracy (Doniach model[40]), we derived exact expressions for the pseudo-critical temperature and residual entropy, revealing how configurational imbalance drives sharp entropy plateaus. In the mixed spin-1/2 and spin-1 hexagonal nanowire, symmetry reduction yielded dominant blocks whose interaction could be described by a small effective matrix. First-order corrections captured the pseudotransition line with excellent accuracy, even as full irreducibility was preserved.

While the emergence of nearly block-diagonal transfer matrices may seem mathematically expected in low-temperature limits, the thermodynamic consequences of such structures, particularly the sharp yet analytic crossovers observed in several theoretical models, have not been previously identified under a general framework. Our approach clarifies how this common spectral structure underlies a wide variety of seemingly isolated or curious behaviors in the literature[12, 13, 14, 15, 24, 25, 26, 37], offering a simple and physically intuitive explanation for pseudotransition phenomena, which in this framework acquire a precise spectral definition through the minimal gap between dominant transfer-matrix eigenvalues.

In summary, pseudotransitions originate not from broken analyticity, but from the interplay of spectral proximity and suppressed coupling within irreducible transfer matrices. Nearly block-diagonal irreducibility thus provides a natural explanation for sharp thermodynamic responses in 1D systems, without contradicting the general absence of phase transitions[3].

Acknowledgments

This work was partially supported by the Brazilian funding agencies CNPq and FAPEMIG.

7. Derivation of pseudo-critical temperature

This appendix provides the algebraic derivation of the pseudo-critical conditions, based on the spectral structure of a two-sector transfer matrix and the behavior of the spectral gap $\zeta(x, T)$.

For simplicity, we assume that each effective matrix element is given by a Boltzmann sum over internal excitations. Assuming the system is gapped, we write,

$$w_\nu(x, T) = g_{\nu,0} e^{-\varepsilon_{\nu,0}(x)/T} \eta_\nu(x, T), \quad (67)$$

with $\nu = \{a, 0, b\}$, where the correction factor is

$$\eta_\nu(x, T) = 1 + \sum_{k=1} \hat{g}_{\nu,k} e^{-\delta_{\nu,k}(x)/T}, \quad (68)$$

where $\hat{g}_{\nu,k} = \frac{g_{\nu,k}}{g_{\nu,0}}$ representing the relative degeneracy of the k -th excited level, and $\delta_{\nu,k}(x) = \varepsilon_{\nu,k}(x) - \varepsilon_{\nu,0}(x)$ being the excitation gap. In the low-temperature limit, we approximate $\eta_\nu(x, T) \approx 1$, neglecting excited-state contributions.

The temperature T and x -derivatives of w_ν , then follow

$$\frac{\partial w_\nu}{\partial T} = \frac{\varepsilon_{\nu,0}}{T^2} w_\nu, \quad \frac{\partial w_\nu}{\partial x} = -\frac{w_\nu}{T} \frac{\partial \varepsilon_{\nu,0}}{\partial x}. \quad (69)$$

Let us define the mean and difference of ground-state energies as $\bar{\varepsilon} = \frac{\varepsilon_{a,0}(x) + \varepsilon_{b,0}(x)}{2}$ and $\varepsilon = \varepsilon_{a,0}(x) - \varepsilon_{b,0}(x)$, both of which depend on x . Then, using the notation in the main text and the result from (69), we compute

$$\frac{\partial \sigma}{\partial T} = \frac{1}{T^2} (\bar{\varepsilon} \sigma + \varepsilon \bar{w}), \quad (70)$$

$$\frac{\partial \bar{w}}{\partial T} = \frac{1}{T^2} \left(\bar{\varepsilon} \bar{w} + \frac{1}{4} \varepsilon \sigma \right), \quad (71)$$

$$\frac{\partial w_0}{\partial T} = \frac{1}{T^2} \varepsilon_{0,0} w_0, \quad (72)$$

Substituting into Eq. (16), the temperature derivative of the spectral gap becomes

$$\frac{\partial \zeta(x, T)}{\partial T} = \frac{\varepsilon \sigma (w_a w_b - w_0^2) + 4(\bar{\varepsilon} - \varepsilon_{0,0}) w_0^2 \bar{w}}{T^2 \bar{w}^2 \sqrt{4w_0^2 + \sigma^2}}. \quad (73)$$

Assuming $x = x_p$ fixed, the anti-crossing (pseudotransition) occurs when $\zeta(x_p, T)$ reaches a minimum at temperature $T = T_p^*$. Therefore, from (73) and (19), the pseudotransition condition results in

$$\varepsilon \sigma (w_a w_b - w_0^2) + 4(\bar{\varepsilon} - \varepsilon_{0,0}) w_0^2 \bar{w} = 0. \quad (74)$$

This expression defines the general pseudo-critical condition in the presence of two competing gapped sectors with weak coupling w_0 . In the low-temperature limit, $w_0 \ll w_a \sim w_b$, and $w_0 \rightarrow 0$ as $T \rightarrow 0$, but remains nonzero for finite T . The sign of σ may vary and even vanish near the crossover, depending on T and x .

A similar condition arises from the derivative with respect to x . Using:

$$\frac{\partial \sigma}{\partial x} = -\frac{1}{T} (\bar{\varepsilon}' \sigma + \varepsilon' \bar{w}), \quad (75)$$

$$\frac{\partial \bar{w}}{\partial x} = -\frac{1}{T} \left(\bar{\varepsilon}' \bar{w} + \frac{1}{4} \varepsilon' \sigma \right), \quad (76)$$

$$\frac{\partial w_0}{\partial x} = -\frac{1}{T} \varepsilon'_{0,0} w_0, \quad (77)$$

where the prime denotes derivative with respect to x , and $\bar{\varepsilon}' = \frac{\varepsilon'_{a,0}(x) + \varepsilon'_{b,0}(x)}{2}$ and $\varepsilon' = \varepsilon'_{a,0}(x) - \varepsilon'_{b,0}(x)$, we obtain, from eq.(16),

the derivative of $\zeta(x, T)$ with respect to x becomes

$$\frac{\partial \zeta(x, T)}{\partial x} = \frac{-\varepsilon' \sigma (w_a w_b - w_0^2) - 4(\bar{\varepsilon}' - \varepsilon'_{0,0}) w_0^2 \bar{w}}{T \bar{w}^2 \sqrt{4w_0^2 + \sigma^2}}. \quad (78)$$

Thus, the anti-crossing occurs when $\zeta(x, T_p)$ reaches a minimum at a specific value x_p . From (78) and (17), this condition leads to the following expression

$$\varepsilon' \sigma (w_a w_b - w_0^2) + 4(\bar{\varepsilon}' - \varepsilon'_{0,0}) w_0^2 \bar{w} = 0. \quad (79)$$

References

- [1] L. Van Hove, *Physica* **16**, 137 (1950). [1](#)
- [2] D. Ruelle, *Comm. math. Phys.* **9**, 267 (1968) [1](#)
- [3] J. A. Cuesta and A. Sanchez, *J. Stat. Phys.* **115**, 869 (2003) [1](#), [2.1](#), [2.1](#), [6](#)
- [4] K. Y. Lin *Chin. Journ. Phys.* **15**, 283 (1977). [1](#), [2.1](#)
- [5] F. Ninio, *J. Phys. A: Math Gen* **9** 1281 (1976) [1](#), [2.1](#)
- [6] D. A. Lavis, *Equilibrium Statistical Mechanics of Lattice Models* (Springer Netherlands, 2015). [1](#), [2.1](#)
- [7] I. M. Carvalho, J. Torrico, S. M. de Souza, M. Rojas, O. Rojas, *J. Magn. Magn. Mats.* **465**, 323 (2018) [1](#)
- [8] L. Galisova and J. Strečka, *Phys. Rev. E* **91**, 022134 (2015) [1](#)
- [9] T. Hutak, T. Krokhmalkii, O. Rojas, S. M. de Souza, O. Derzhko, *Phys. Lett. A* **387**, 127020 (2021) [1](#)
- [10] J. Lee and J. M. Kosterlitz, *Phys. Rev. B* **43**, 3265 (1991) [1](#)
- [11] P. N. Timonin, *J. Exp. Theor. Phys.* **113**, 251 (2011) [1](#)
- [12] S. M. de Souza and O. Rojas, *Sol. Stat. Comm.* **269**, 131 (2017) [1](#), [2.3.1](#), [3.1.1](#), [3.1.1](#), [6](#)
- [13] W. Yin and A. M. Tselik, *Phys. Rev. Lett.* **133**, 266701 (2024) [1](#), [2.3.1](#), [3.1.1](#), [6](#)
- [14] W. Yin, *Phys. Rev. B*, **109**, 214413 (2024) [1](#), [2.3.1](#), [3.1.1](#), [6](#)
- [15] W. Yin, *Phys. Rev. Research* **6**, 013331 (2024) [1](#), [2.3.1](#), [3.1.1](#), [6](#)
- [16] W. Yin, arXiv:2505.02303 [1](#)
- [17] J. Sznajd, *Phys. Rev. E* **111**, 024117 (2025) [1](#)
- [18] J. Sznajd, *J. Stat. Mech.* 023402 (2022) [1](#)
- [19] O. Rojas, J. Strečka, M. L. Lyra, S. M. de Souza, *Phys. Rev. E* **99**, 042117 (2019). [1](#)
- [20] O. Rojas, *Chin. Jour. Phys.* **70**, 157 (2021) [1](#)

- [21] O. Rojas, Braz. Jour. Phys. 50 (2020) 675; Acta Phys. Pol. A **137**,933 (2020). [1](#), [3.2.1](#)
- [22] D. Yasinskaya, Y. Panov, Phys. Rev. E **110**, 044118 (2024). [1](#)
- [23] I. M. Carvalho, J. Torrico, S. M. de Souza, O. Rojas, O. Derzhko, Ann. Phys. **402**, 45 (2019) [1](#)
- [24] T. Krokhmalkskii, T. Hutak, O. Rojas, S. M. de Souza, O. Derzhko, Physica A **573**, 125986 (2021). [1](#), [2.3.1](#), [3.1.1](#), [6](#)
- [25] Y. D. Panov and O. Rojas, Phys. Rev. E **103**, 062107 (2021) [1](#), [2.3.1](#), [3.1.1](#), [4](#), [6](#)
- [26] J. Chapman, B. Tomasello and S. Carr, J. Stat. Mech. 093214 (2024). [1](#), [2.3.1](#), [3.1.1](#), [6](#)
- [27] T. F. Lourenço, <https://doi.org/10.11606/D.43.2021.tde-13092021-120600> [1](#), [4](#), [4.2](#), [4.2](#), [4.2](#)
- [28] J. Strečka, *Pseudo-Critical Behavior of Spin-1/2 Ising Diamond and Tetrahedral Chains*, in: *An Introduction to the Ising Model*, Ed. S. Luoma, Nova Science Publishers, New York, 2020, pp. 63-86, Chapter 4. [1](#)
- [29] J. Strečka, Acta Phys. Pol. A, **137**, 610-612 (2020) [1](#)
- [30] O. Rojas, J. Strečka and S.M. de Souza, Sol. Stat. Comm. **246**, 68 (2016) [1](#)
- [31] D. Yasinskaya, Y. Panov, arXiv:2401.15087v1 [1](#)
- [32] Y. Panov, *Phys. Rev. E* **106**, 054111 (2022). [1](#)
- [33] O. Rojas, J. Strečka, O. Derzhko, S. M. de Souza, Jour. Phys.: Condensed Matter **32**, 035804 (2019) [1](#)
- [34] J. Strečka, R. C. Alecio, M. Lyra and O. Rojas, J. Magn. Magn. Mats. **409**, 124 (2016) [1](#)
- [35] O. Rojas, and S. M. de Souza, J. Torrico, L.M. Verissimo, M. S. S. Pereira, M. L. Lyra, Phys. Rev. E **103**, 042123 (2021). [1](#)
- [36] O. Rojas, S. M. de Souza, J. Torrico, L. Verissimo, M. S. S. Pereira, M. L. Lyra, and O. Derzhko, Phys. Rev. E **110**, 024130 (2024). [1](#)
- [37] J. Strečka, K. Karlova, Eur. Phys. J. B **97**, 74 (2024) [1](#), [2.3.1](#), [3.1.1](#), [6](#)
- [38] R. A. Pimenta, O. Rojas, S. M. de Souza, J. Mag. Mat. Mag, **550**, 169070 (2022) [1](#), [5](#), [5.1](#), [5.2](#), [5.2.2](#)
- [39] Y. D. Panov and O. Rojas, Phys. Rev. E **108**, 044144 (2023). [1](#)
- [40] S. Doniach, J. Chem. Phys. **68**, 4912 (1978) [1](#), [4](#), [4.1](#), [6](#)
- [41] H. A. Kramers, G. H. Wannier, *Statistics of the Two-Dimensional Ferromagnet. Part I*, Phys. Rev. **60**, 252 (1941); *Statistics of the Two-Dimensional Ferromagnet. Part II*, Phys. Rev. **60**, 263 (1941). [2](#)
- [42] T.Kato, *Perturbation Theory for Linear Operators* (Springer,Berlin,1995). [2.1](#), [2.1](#), [3.1](#)
- [43] C. Kittel, Am. J. Phys. **37**, 917(1969) [2.2](#)
- [44] L. D. Mosgaard, A. D. Jackson, and T. Heimburg, J. Chem. Phys. **139**, 125101 (2013) [4](#)
- [45] A. V. Badasyan, A. Giacometti, Y. S. Mamasakhlisov, V. F. Morozov, and A. S. Benight, Phys. Rev. E **81**, 021921 (2010) [4](#)
- [46]] I. Syozi, Prog. Theor. Phys. **6**, 341 (1951); M. Fisher, Phys. Rev. **113**, 969 (1959); O. Rojas, J. S. Valverde, S. M. de Souza, Physica A **388**, 1419 (2009); J. Strečka, Phys. Lett. A **374**, 3718 (2010); O. Rojas, S. M. de Souza, J. Phys. A: Math. Theor. **44**, 245001 (2011) [4](#)
- [47] P. Lv, Y. Zhang, R. Xu, J-C Nie, L. He, J. Appl. Phys. **111**, 013910, (2012) [5](#)
- [48] X. Yuan, C. Du, G. Sun, N. Pan, Appl. Surf. Sci. **253**, 4546 (2007) [5](#)
- [49] Z. Yang, Z. Li, L. Liu, L. Kong, J. Magn. Magn Mater. **323**, 2674 (2011) [5](#)
- [50] R. Masrour, A. Jabar, A. Benyoussef, M. Hamedoun, L. Bahmad, Phys. B **472**, 19 (2015) [5](#)
- [51] M. Ertas and E. Kantar, Commun. Theor. Phys. **64**, 401 (2015) [5](#)
- [52] R. G. B. Mendes, F. C. Sá Barreto, J. P. Santos, Braz. J. of Phys. **48**, 137 (2018); Physica A **505**, 1186 (2018); [5](#), [5.2](#), [4](#), [5.2.1](#)